AIAA JOURNAL
Vol. 32, No. 6, June 1994

Computation of Separated Duct Flows Using the Boundary-Layer Equations

V. I. Vasilev*
Central Institute of Aviation Motors, Moscow, Russia

A semi-inverse method, based on boundary-layer equations, for simulation of duct flows with strong viscous/inviscid interaction is developed. An improved interaction formula, based on the matching of parameters in viscous and inviscid zones, is proposed. Using this method the laminar and turbulent flows in plane channels, swirl flow in annular channels, and a bypass flow with downstream mixing of the trailing edge of a splitter were calculated. The results for the plane channel and bypass flows are in good agreement with known experimental and theoretical data. The influence of swirl and parameters of the bypass flow on the separation zone structure were investigated. A new type of self-similar solution for swirl boundary-layer equations was obtained.

Nomenclature

c	= mass concentration
h	= duct height
i	= iteration number
k	= turbulence model coefficients
L	= characteristic length
m	= velocity ratio
n	= density ratio
p	= pressure
Re	= Reynolds number, $u_0 L/\nu$
r	= wall coordinate
Sc	= Schmidt number
U, V	= velocity components in boundary layer
u, v	= velocity components in inviscid core
w	= swirl velocity
X, Y	= boundary-layer coordinates
x, y	= coordinates (Cartesian or cylindrical)
α	= deflected angle
β	= pressure gradient
Γ	= circulation
γ	= swirl parameter
δ^*	= displacement thickness
ζ	= relaxation parameter
η	= transformed coordinate
ν	= laminar viscosity
ν_t	= turbulent viscosity
ρ	= density
τ	= shear stress
Φ, ψ	= stream functions

Subscripts

d	= below splitter
e	= boundary-layer edge
o	= duct entrance
te	= trailing edge
u	= above splitter
w	= on the wall
$+$	= upper wall
$-$	= lower wall

Received Sept. 15, 1992; revision received Nov. 15, 1993; accepted for publication Nov. 15, 1993.

*Head of Group, Aviamotornaya St., 2.

Introduction

THE solution of direct boundary-layer problems (with a prescribed pressure distribution) cannot be continued downstream of a separation point due to Goldstein's singularity. Catherall and Mangler[1] showed that by solving the inverse problem for the boundary-layer equations (with a prescribed displacement thickness) one can calculate a flow with recirculation zones. Carter[2] proposed the interaction algorithm allowing the calculation of the flow around a given surface using this approach. Since then such approaches have been widely used. The most common applications were the flows around profiles, including those with trailing-edge and leading-edge separation. Other examples can also be found; see, for example Refs. 3 and 4.

In the present work the boundary-layer equations were used to calculate incompressible separated duct flows. These flows include laminar and turbulent flows in plane channels, swirl flows, and bypass flows with mixing downstream of the trailing edge of a splitter.

The strong viscous/inviscid interaction in a separation region was simulated using a so-called semi-inverse method. The flow in the duct was divided into thin viscous zones, including wall boundary layers and a mixing zone downstream of the splitter, and the inviscid cores. To describe the flow in the viscous zones, the inverse problems (with prescribed displacement thicknesses) were solved. To find the flow in the inviscid core, the direct problem (with the prescribed wall's contour corrected by displacement thickness) was considered. The linear theory or numerical integration may be used for solving this problem. Then the interaction algorithm was used to solve for the distributions of displacement thicknesses, allowing satisfaction of the matching conditions. The simple interaction algorithm developed by Carter was tried and this led to an improved interaction formula, which is a reasonable compromise between Carter's method and Veldman's quasisimultaneous method.[5]

The presented results increase to some extent the area of application of interaction boundary-layer algorithms.

Plane Duct Flows

Boundary-Layer Simulation

First the incompressible flow of a fluid in a plane duct was considered. A schematic of the flow is presented in Fig. 1a. The wall contours are described by functions $y = r_+(x)$ (upper wall) and $y = r_-(x)$ (lower wall), where x and y are Cartesian coordinates. The Reynolds number considered is large, so that near the duct entrance the boundary-layer displacement thickness is much smaller than the duct width [$\delta^* \ll (r_+ - r_-)$] and

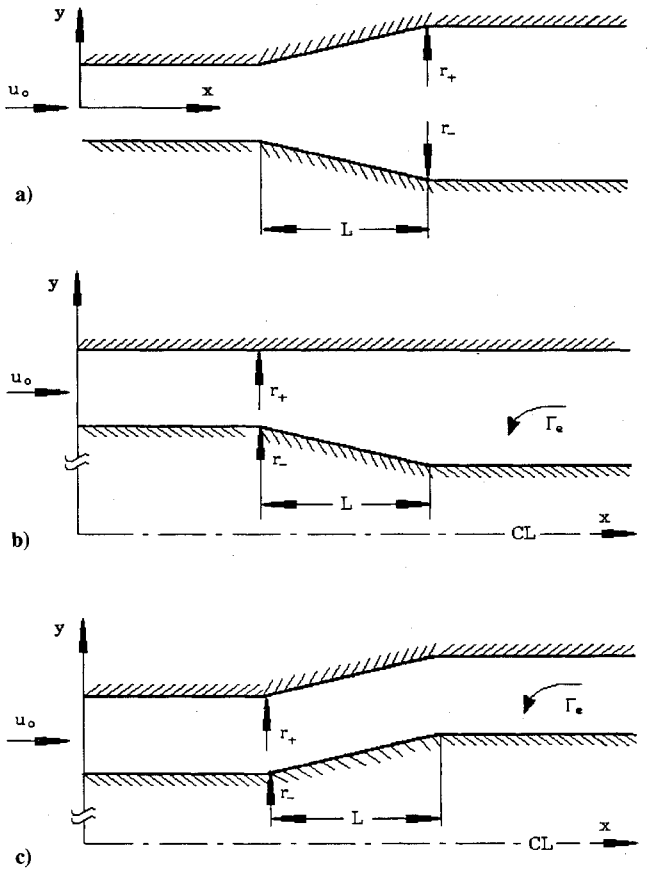

Fig. 1 Schematic diagram of a) planar diffuser, b) annular convergent, and c) S-shaped ducts.

only the flow in this region is simulated. If the duct is a diffuser, then contour variations considered are small $\Delta r \sim dr/dx \sim \mathcal{O}(\delta^*)$, i.e., only the flows with thin separation regions are investigated. The latter restriction allows the use of linear theory for prediction of the inviscid core. A one-equation turbulence model is used in the analysis.

It is convenient to write the boundary-layer equations using a transformation of variables:

$$X = x, \quad Y = \mp[y - r_\pm(x)], \quad U = u, \quad V = \mp(v - u \cdot dr_\pm/dx)$$

where u and v are the velocity components in the Cartesian coordinates. In the transformed variables, however, the equations have the usual form

$$\rho U \frac{\partial U}{\partial X} + \rho V \frac{\partial U}{\partial Y} = \beta + \frac{\partial}{\partial Y}\left[\rho(\nu + \nu_t)\frac{\partial U}{\partial Y}\right] \tag{1}$$

$$\frac{\partial \rho V}{\partial Y} = -\frac{\partial \rho U}{\partial X} \tag{2}$$

where

$$\beta = \rho U_e \frac{dU_e}{dX}, \qquad U_e = \lim_{Y\to\infty} U(X, Y)$$

is the velocity at the outer edge of the boundary layer. Density is constant here.

Turbulent viscosity in this work is found using the one-equation model[6]

$$\rho U \frac{\partial \nu_t}{\partial X} + \rho V \frac{\partial \nu_t}{\partial Y} = \frac{\partial}{\partial Y}[\rho(k_1\nu_t + \nu)]\frac{\partial \nu_t}{\partial Y} + k_2\rho\nu_t\left|\frac{\partial U}{\partial Y}\right| - k_3\rho\nu_t(k_4\nu_t + \nu)/Y^2 \tag{3}$$

where empirical coefficients are taken from Ref. 6 and $k_1 = 2.0$, $k_3 = 50.0$, $k_4 = 0.06$, and $k_2 = 0.2[(\nu_t/8\nu)^2 + 1.4(\nu_t/8\nu) + 0.2]/[(\nu_t/8\nu)^2 - 1.4(\nu_t/8\nu) + 1.0.]$ Boundary conditions for Eqs. (1-3) have the form

$$Y = 0, \quad U = V = \nu_t = 0; \quad Y \to \infty \quad \frac{\partial U}{\partial Y} \to 0 \quad \frac{\partial \nu_t}{\partial Y} \to 0 \tag{4}$$

Initial conditions are given by

$$U(X_o, Y) = U_o f(Y), \qquad \nu_t(X_o, Y) = U_o \delta_o^* g(Y) \tag{5}$$

When a laminar boundary layer was considered, $g = 0$, and f was found from the Blasius solution. In the turbulent case, f and g were taken to be the same as in a turbulent boundary layer on a flat plate.[7]

For a direct boundary-layer problem, β is a known function. For the inverse problem, this parameter is unknown and to find it one must specify the displacement thickness, i.e., β is determined by the condition

$$\int_0^\infty (1 - \rho U/\rho_e U_e)\, dY = \delta^*(X) \tag{6}$$

Equations (1-3) with boundary conditions (4) and (5) were solved numerically by a marching finite difference method. Equations (1) and (3) were approximated by a central-difference second-order scheme in the Y direction and an upwind first-order scheme in the X directions. The scheme is implicit, and to resolve the nonlinear terms local iteration at each X station was utilized. To approximate the convection term $U(\partial U/\partial X)$ in the reverse flow zone, either the FLARE approximation[8] or an upwind scheme were used. In the upwind scheme, the parameters at downstream stations were taken from the previous iteration of the global iteration procedure. The FLARE approximation was used only in some test cases where the pure inverse problem for the boundary-layer equations was solved. Our experience showed that if velocity in the reverse flow zone is less than $0.1U_e$, the results obtained by the two methods are practically the same (the difference is smaller than 1%). In the other cases, the upwind scheme gave more precise results, which might even differ quantitatively from the results obtained with the help of FLARE. (For instance, FLARE did not yield two vortices in the recirculation region.)

The integral in Eq. (6) was approximated by the trapezoidal formula, and by the same method Eq. (2) was integrated to find V.

The system of algebraic equations corresponding to Eq. (3) had a tridiagonal matrix and was solved by an efficient tridiagonal martrix algorithm (TDA) method. Equation (1) was solved simultaneously with the integral condition (6) to find u and β. The corresponding system of algebraic equations had a tridiagonal matrix with one full string and was solved by a slightly modified TDA method.

The finite difference grid in the Y direction was nonuniform with grid nodes condensed to the wall according to Blottner's recommendations[9]

$$Y_j = Y_N(1.82^{\frac{j-1}{N-1}10} - 1)/(1.82^{10} - 1) \qquad j = 1 \ldots N$$

where j is the number of the node and Y_N the boundary of the computational domain at a given X station. Except near the trailing edge of the splitter, the grid in the X direction was homogeneous. According to test calculations, a grid with 60 nodes in the Y direction and 100 nodes in the X direction was dense enough to get about 1% accuracy.

The one-equation turbulence model[6] was initially constructed for attached flow. As our previous investigation showed,[10] it also gave reasonable results for separated flows. Some illustrations are shown in Fig. 2, where a comparison of computed velocity, shear stress profiles, and experimental data[11] are presented. The computational results presented here were obtained as the solution of the inverse boundary-layer

problem with prescribed δ^* taken from experiment. Characteristic length L is the distance between the entrance of the experimental model and the last station at which measurements were taken.

Potential Core

Parameters in the boundary layer must be matched with parameters in the inviscid core. Only flows where the core is a potential flow are considered. Thus, if a stream function Φ is used, it must satisfy the Laplace equation for an incompressible flow. Generally, this equation in a domain with curvilinear boundaries may be integrated numerically. However, using the assumption that wall contour variations are small, one can obtain an analytical solution. More precisely, these assumptions are that the contour variations are small $[\Delta r_+ \sim \Delta r_- \sim dr_+/dx \sim dr_-/dx = \mathcal{O}(\epsilon)$, where ϵ is small parameter], and that the walls of the entrance and exit parts of the duct are parallel to the x axis, i.e., $dr_+/dx = dr_-/dx = 0$ if $x < x_L$ or $x > x_R$. In this work only ducts that satisfied these restrictions were considered.

Using transformed coordinates x, $\eta = (y - r_-)/h$, and $h = r_+ - r_-$, and representing the stream function as $\Phi = u_o h_o (\eta + \psi)$ (in the case considered here the duct entrance is located at $x \to \infty$), one can obtain the equation and boundary conditions, which the stream function must satisfy to the order of $0(\epsilon^2)$. These relations are:

$$\frac{\partial^2\psi}{\partial x^2} + (1/h_o^2)\frac{\partial^2\psi}{\partial\eta^2} = (1/h_o)\left[(1-\eta)\frac{d^2r_-}{dx_-^2} + (\eta)\frac{d^2r_+}{dx_+^2}\right]$$
$$\psi(x, 0) = \psi(x, 1) = 0, \qquad \psi(\mp\infty, \eta) = 0 \tag{7}$$

This problem is solved using the Fourier transform. According to this solution, the longitudinal velocity at the lower wall is given by

$$u(x, y = r_-) = u_o(h_o/h)\left\{1 + (1/\pi h_o)\int_{-\infty}^{\infty}\left[K\left(\frac{x-\xi}{h_o}\right)\frac{dr_-}{d\xi} + K_1\left(\frac{x-\xi}{h_o}\right)\frac{dr_+}{d\xi}\right]d\xi\right\} \tag{8}$$

where K and K_1 have the form

$$K(z) = (\pi/2)\left[cth\left(\frac{\pi z}{2}\right) - 1\right] \quad \text{if} \quad z > 0,\ K(-z) = K(z)$$
$$K_1(z) = (\pi/2)\left[1 - th\left(\frac{\pi z}{2}\right)\right] \quad \text{if} \quad z > 0,\ K_1(-z) = K_1(z)$$

To find the velocity at the upper wall of the duct one must replace $dr_-/d\xi$ and $dr_+/d\xi$ in relationship (8). The integrals were calculated numerically using the trapezoidal formula.

Interacting Algorithm

If the velocity in the potential core with the wall corrected by the displacement thickness is named u_e [for instance, on the lower wall $u_e = u\ (x, y = r_- + \delta^*)$], then the matching condition may be written as follows:

$$U_e(x) = u_e(x) \tag{9}$$

It can be easily shown that condition (9) also assures the matching of cross velocities.

Equation (9) enables a solution to be found for δ^*, but the relation of U_e and u_e with δ^* is implicit, and therefore the interaction algorithm must be exploited. As a first possibility we used Carter's formula

$$\delta^{*i+1}/\delta^{*i} = 1 + \zeta\left(\frac{u_e - U_e}{U_e}\right)^i \tag{10}$$

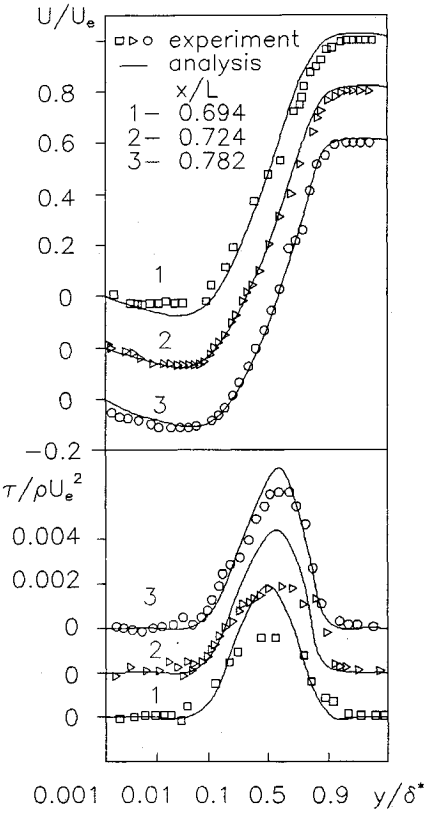

Fig. 2 Comparison of calculated and measured mean velocity and Reynolds shear stress profiles.

As a second possibility, a more elaborate algorithm was constructed.

According to linear theory, the potential flow velocity on a free surface with contour $y = r + \delta^*$ is given by

$$u_e = u_o\left[1 + (1/\pi)\int_{-\infty}^{\infty} -\frac{d(r+\delta^*)}{d\xi}\frac{d\xi}{x-\xi}\right]$$

It should be noted that this simple relation was used instead of Eq. (8) because of the approximate character of the interaction formula. Replacing the integral by a finite difference expression one can obtain

$$(\Delta u_e)_m = \sum_j C_{mj}\Delta\delta^* j \tag{11}$$

where $\Delta u_e = u_e^{i+1} - u_e^i$, $\Delta\delta^* = \delta^{*i+1} - \delta^{*i}$, j, m grid points locations.

Using von Kármán's equation, one can also obtain the approximate relation between increments of U_e and δ^*

$$\Delta U/U = -(\Delta\delta^*/\delta^*)\,[1/(2+H)] \tag{12}$$

where H is a shape factor. Subtracting Eq. (12) from Eq. (11) and supposing $u_e^{i+1} = U_e^{i+1}$, one can find

$$(u_e - U_e)_m^i = \sum_j \Gamma_{mj}\Delta\delta_j^* \tag{13}$$

When the system (13) is solved, the new distribution of δ^* may be calculated as

$$\delta^{*i+1} = \delta^{*i} + \zeta\Delta\delta^*$$

A comparison of the convergence of algorithms (10) and (13) is shown in Fig. 3. The convergence history for a laminar boundary layer in a symmetrical diffuser (for more detail see the following) is presented. Carter's formula with the largest possible relaxation parameter is slower to converge than is formula (13).

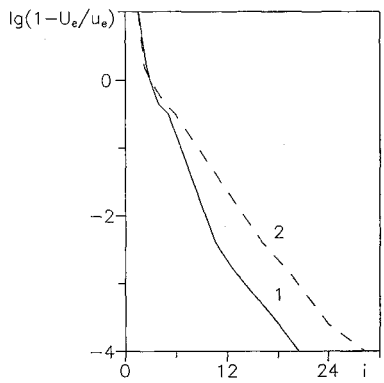

Fig. 3 Convergency hierarchy of interacting procedure: 1) present algorithm and 2) Carter's technique.

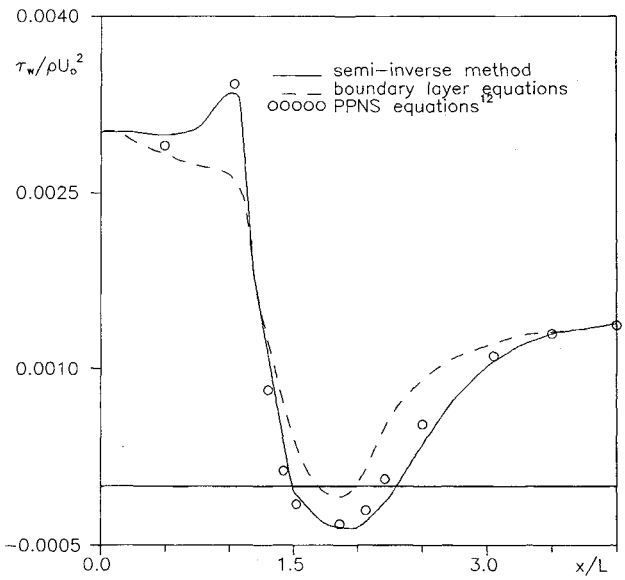

Fig. 4 Wall shear stress distribution in the planar symmetrical diffuser (laminar flow).

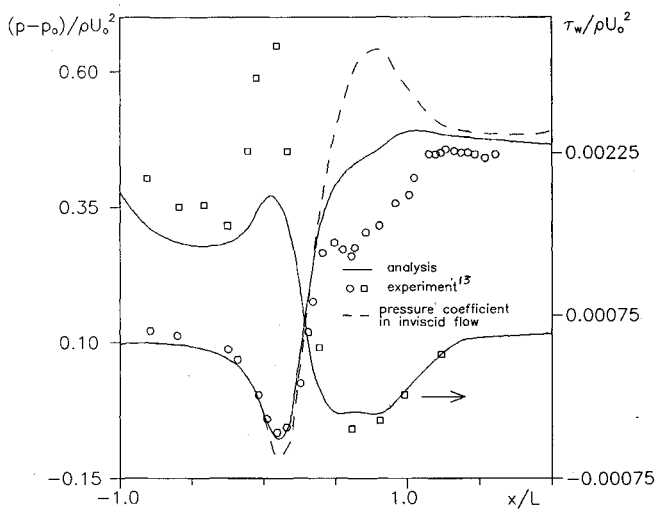

Fig. 5 Shear stress and pressure coefficient distributions along the curved wall of the planar diffuser (turbulent flow).

Calculation Results

The method is demonstrated by means of two examples: 1) laminar flow in a symmetrical diffuser, calculated earlier by Halim and Hafez[12] using partially parabolized Navier-Stokes equations, and 2) turbulent flow in a diffuser, experimentally investigated by Serpa et al.[13]

Symmetrical diffuser walls are given by $r_- = -r_+$, $r_+(x)/L = 1 + 0.08(x^o - 1)^2 (5 - 2x^o)$ if $1 \le x^o \le 2$, $r_+/L = 1$, $x^o \le 1$, and $r_+/L = 1.08$, $x^o \ge 2$, where L is the length of the divergent part $x^o = x/L$. $Re = 6.25 \times 10^3$, the origin of the laminar boundary layer, was placed at $x^o = -1.96$ ($x = 0$ is the entrance of the calculation domain).

The wall shear stress distribution is presented in Fig. 4. There is a thin separation region in the divergent section of the diffuser. Our results are in good agreement with results by Halim and Hafez,[12] also shown in Fig. 4. The wall shear stress distribution is also presented in Fig. 4 using the assumption that the pressure across the channel is uniform and the flow is simulated by the boundary-layer equations, i.e., the viscous/inviscid interaction is not taken into account. The latter results differ from the results that account for the viscous/inviscid interaction rather significantly.

Other diffuser walls are given by $r_+/L = 0.75$, $r_-(x)/L = 0.201 - 1.981(x^o)^3 + 2.956(x^o)^4 - 1.176(x^o)^5$ if $0 \le x^o \le 1$, $r_-/L = 0.201$ $x^o \le 0$, and $r_-/L = 0$ $x^o > 1$. $Re = 5.85 \times 10^5$, the origin of the turbulent boundary layer was placed at $x^o = -2.7$ ($x = -1$ is the entrance of the calculation domain).

The pressure coefficient and shear stress along the curved wall are presented in Fig. 5. In the separation region, the wall shear stress is in good agreement with experimental data.[13] The calculated pressure coefficient is significantly less than that in an inviscid flow, but still well above the experimental data. To increase the accuracy of the simulation, the turbulence model must be improved. Overall, the agreement is thought to be good.

Swirl Flow

Boundary-Layer Simulation

The viscous/inviscid interaction method can also be used to simulate some swirling flows. Consider the swirling flow of an incompressible fluid in an annular duct, such as that presented in Figs. 1b and 1c. All preceding restrictions are assumed, and, in addition, $r_\pm \gg r_+ - r_-$. The boundary layers are described by the same equations if the weaker additional restriction $r_- \ge r_+ - r_-$ is satisfied, but the strong condition is a simplification of the inviscid core simulation. If the inviscid core is calculated numerically, then the strong restriction is not needed.

Under the aforementioned assumption, the momentum equations in the longitudinal and cross directions in the boundary layer with swirl are written as follows

$$U\frac{\partial U}{\partial X} + V\frac{\partial U}{\partial Y} = \frac{\Gamma^2}{r_\mp^3}\left(\frac{dr}{dX}\right)_\mp - \frac{1}{\rho}\frac{\partial p}{\partial X} + \frac{\partial}{\partial Y}\left[(\nu + \nu_t)\frac{\partial U}{\partial Y}\right] \quad (14)$$

$$\frac{1}{\rho}\frac{\partial p}{\partial Y} = \pm\frac{\Gamma^2}{r_\mp^3}\left(\frac{dr}{dX}\right)_\mp \quad (15)$$

where $\Gamma = w \cdot y$, and other notations are the same as in Eq. (1). External to the boundary layer, relationships (14) and (15) are reduced to

$$\frac{1}{\rho}\frac{\partial p_e}{\partial X} = -U_e\frac{dU_e}{dX} + \frac{\Gamma^2}{r_\mp^3}\left(\frac{dr}{dX}\right)_\mp \quad (16)$$

$$\frac{1}{\rho}\frac{\partial p_e}{\partial Y} = \pm\frac{\Gamma^2}{r_\mp^3}\left(\frac{dr}{dX}\right)_\mp \quad (17)$$

If the swirl is small or modest ($\Gamma/U/r \le 1$), then according to Eqs. (15) and (17) pressure variation across the boundary layer is $\mathcal{O}(Re^{-1/2})$ and can be neglected, i.e., one can suppose $p = p(X)$. If the swirl is too large ($\Gamma/U/r > \text{const}\, Re^{-1/4}$), then

our analysis shows (for example, see the following analysis of a self-similar solution) that the separated flows cannot be simulated by the boundary-layer equations. In the intermediate region $1 \ll \Gamma/U/r \ll Re^{1/4}$, cross-stream pressure variations must be included and, according to Eqs. (15) and (17), the pressure at any station is given by

$$p = p_e(X) \pm \rho \int_Y^\infty (\Gamma^2 - \Gamma_e^2)/r_\mp^3 \, dY \tag{18}$$

Substituting Eqs. (18) and (16) into Eq. (14) one can get the longitudinal momentum equation. The full set of equations for an incompressible boundary layer with a swirl are written as follows

$$U\frac{\partial U}{\partial X} + V\frac{\partial U}{\partial Y} = \beta + \frac{\Gamma^2 - \Gamma_e^2}{r_\mp^3}\left(\frac{dr}{dX} \mp\right)$$
$$\pm \frac{\partial}{\partial X}\left[\int_Y^\infty \frac{(\Gamma^2 - \Gamma_e^2)}{r_\mp^3} dY\right] + \frac{\partial}{\partial Y}\left[(\nu + \nu_t)\frac{\partial U}{\partial Y}\right] \tag{19}$$

$$U\frac{\partial \Gamma}{\partial X} + V\frac{\partial \Gamma}{\partial Y} = \frac{\partial}{\partial Y}\left[(\nu + \nu_t)\frac{\partial \Gamma}{\partial Y}\right] \tag{20}$$

$$\frac{\partial U}{\partial X} + \frac{\partial V}{\partial Y} = 0 \tag{21}$$

In this work we consider only a laminar flow ($\nu_t = 0$). Boundary and initial conditions for Eqs. (19) and (21) are the same as those for Eqs. (1) and (2). The closure relation has form (6), and boundary conditions for Eq. (20) may be written as

$$Y = 0, \quad \Gamma = 0, \quad Y \to \infty \; \Gamma \to \Gamma_e, \quad \Gamma(X_0, Y) = \Gamma_e \cdot f(Y) \tag{22}$$

where Γ_e is the prescribed value.

Before the viscous/inviscid interaction in the swirl flow is analyzed, it is useful to discuss some self-similar solutions of Eqs. (19–21).

Self-Similar Solutions of Swirling Boundary-Layer Equations

Some authors earlier investigated the self-similarity characteristic of boundary layers with swirl with uniform pressure across the layer, i.e., when the integral term on the right-hand side of Eq. (19) is negligible (for example, see Ref. 14). Here this term is included, but rather exotic power distributions of swirl ($\Gamma_e \sim X^m$) are not considered and only free vortex swirl ($\Gamma_e = \text{const}$) is analyzed. Under this restriction, self-similarity is possible only if $r = \text{const}$, $U_e = U_o X^{1/5}$. However, one can obtain more general results by supposing that $r = r_o + r_1 X^{2/5}$ and that the variable part is much smaller than the constant ($r_1 X^{2/5} \ll r_o$).

The velocity components of self-similar flow are given by

$$U = U_e(x) f'(\eta), \quad V = -\frac{\sqrt{3/5 U_o \nu}}{X^{2/5}}(f - 2/3\eta f'), \quad \Gamma = \Gamma_e F(\eta)$$

where $\eta = \sqrt{3/5 U_o/\nu}\,(Y/X^{2/5})$. Functions f and F are satisfied by the following equations and boundary conditions

$$f''' + ff'' + \tfrac{1}{3}(1 - f'^2) + \gamma_o\left[\int_\eta^\infty (F^2 - 1)\, d\eta + (F - 1)^2\eta\right]$$
$$+ \gamma_1(F^2 - 1) = 0 \tag{23}$$

$$F'' + fF' = 0 \tag{24}$$

$$f(0) = f'(0) = F(0) = 0, f'(\infty) = F(\infty) = 1 \tag{25}$$

where

$$\gamma_o = \pm 2/3 \frac{\Gamma_e^2}{r_o^3 U_o^2}\sqrt{\nu/(3/5)/U_o}; \qquad \gamma_1 = 2/3 \frac{\Gamma_e^2 r_1}{r_o^3 U_o^2}$$

Parameter γ_o is used to characterize the swirl influence on the boundary layer on a cylindrical surface. This parameter is positive for the flow on the outer side of the surface (lower wall in the annular duct) and negative for the inner side (upper wall in the annular duct). Consequently, the swirl will accelerate the flow near the upper wall and decrease the speed near the lower wall. Parameter γ_1 is used to characterize the swirl influence on the boundary layer on an inclined surface. If the wall is near to the axis ($\gamma_1 < 0$) the flow is accelerated, if it is moved away from the axis ($\gamma_1 > 0$) the speed is decreased.

The range of positive γ_o and γ_1 must be confined, and to find these limits two cases were considered: $\gamma_1 = 0$, $\gamma_o > 0$ and $\gamma_1 > 0$, $\gamma_o = 0$. Equations (23–25) were solved numerically by the method analogous to the one described earlier. Instead of δ^*, the value of parameter $\int_0^\infty (1 - f')\, d\eta$ was prescribed. The relations of $\tau_W = f''(0)$ via γ_o or γ_1 are plotted in Fig. 6, where τ_W is a parameter proportional to wall shear stress. For comparison, the well-known curve $\tau_W(\beta)$, where β is the Faulkner-Skan parameter, is presented. A self-similar solution exists if $\gamma_0 \le 0.265$ or $\gamma_1 \le 0.660$. In the range between zero and the critical value, two solutions exist: one with a reverse flow zone and one without. Qualitatively these solutions are similar to the Faulkner-Skan solutions.

The γ parameters are estimated as

$$\gamma_o \sim \left(\frac{\Gamma_e}{U_e r_o}\right)^2 \frac{L}{r_o}\sqrt{Re_o}, \qquad \gamma_1 \sim \left(\frac{\Gamma_e}{U_e r_o}\right)^2 \frac{\Delta r}{r_o}$$

so that if $r_o = \mathcal{O}(L)$ and $\Delta r = \mathcal{O}(\delta^*)$, the swirl intensity must be limited.

$$\Gamma_e/U_o/r_o \le \text{const}\, Re^{1/4} \tag{26}$$

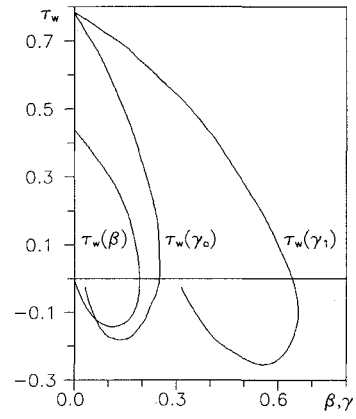

Fig. 6 Self-similar solutions for swirl flows.

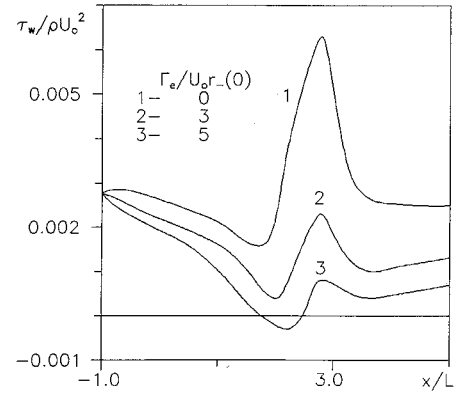

Fig. 7 Shear stress distribution along the curved wall of the annular convergent duct (laminar swirl flow).

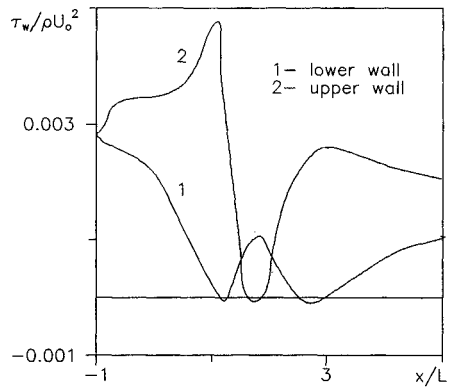

Fig. 8 Wall shear stress distribution in the S-shaped annular duct (laminar swirl flow).

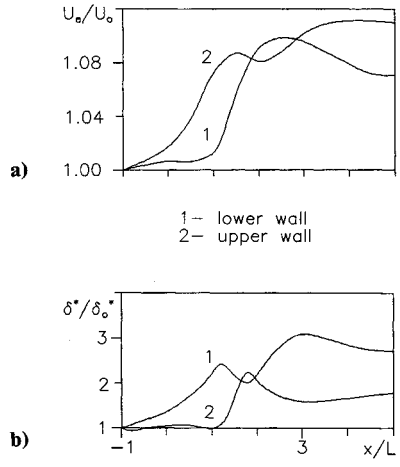

Fig. 9 Distributions in S-shaped annular duct (laminar swirl flow): a) velocity and b) displacement thickness.

With this limitation, the swirl generates a positive pressure gradient. In a duct, the latter condition always occurs near the bottom wall, so the inequality (26) restricts the free vortex swirl in a duct.

Viscous/Inviscid Interaction

The semi-inverse method for swirling flow in a duct is similar to the method just described. Only slight modifications are required to numerically integrate the swirling boundary layer equations (19-21), which contain the additional terms on the right-hand side of Eq. (19) and the equation for the swirl velocity (20). These modifications are obvious.

In this work only free vortex swirl was considered, so the flow in the inviscid core is a potential flow. Additionally, consider only a thin annular duct, where $r_{\pm} \gg r_+ - r_-$. As our investigations have shown, if the annular duct is characterized by the condition $(r_+ - r_-)/r_- \geq 10$, then a numerically calculated velocity distribution differs from the velocity, obtained using formula (8), for the planar duct by less than 1%. Thus, the inviscid core for a swirling flow may be simulated in the same way as in a planar duct.

To find the displacement thicknesses the interaction algorithm (13) was used.

To illustrate the method, the laminar swirl flows in both convergent (Fig. 1b) and S-shaped (Fig. 1c) channels were considered. In both cases the contour of the lower wall is given by $r_-(x)/L = 10 + 0.08(x^o - 2)^2\,(5 - 2x^o)$ if $2 \leq x^o \leq 3$, $r_-/L = 10$ $x^o \leq 2$, $r_-/L = 10.08$ $x^o \geq 3$, and $r_+/L = 11$ for the convergent channel and $r_+/L = r_-/L + 1$ for the S-shaped channel. The initial conditions for longitudinal velocity and Reynolds number were the same as in the case of the plane diffuser described earlier. The swirl intensity Γ_e was varied, and the initial Γ distribution was similar to the longitudinal velocity, i.e., at $x = 0$, $u/u_o = \Gamma/\Gamma_e$.

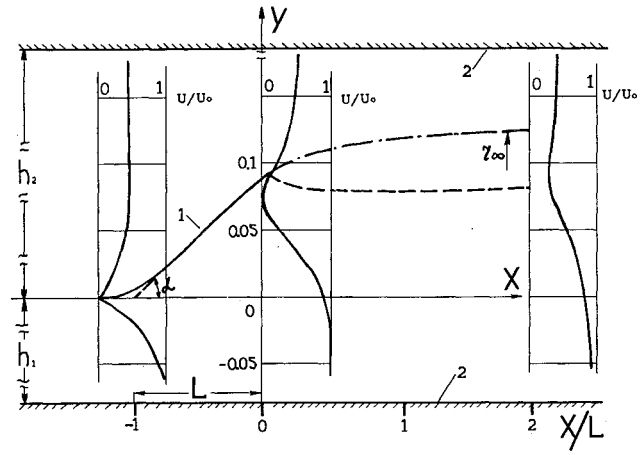

Fig. 10 Schematic diagram of bypass flow, velocity profiles, and positions of dividing streamlines: 1) deflected flap and 2) duct walls.

The wall shear stress distributions along the lower wall of convergent channel for various Γ_e are presented in Fig. 7. These data indicate that without the swirl there is no separation, because the area of the channel cross section diminishes. When the swirl intensity increases the separation zone appears.

The next example corresponds to the S-shaped channel flow at $\Gamma_e/u_o/r_-(0) = 3$. The wall shear stress distributions are presented in Fig. 8. Two separation zones on the lower wall are predicted. The first is due to the wall slope, but the second is in the cylindrical part of the channel. The local acceleration of the flow between these two zones is due to the wall curvature. The upper wall also separates, but only one separation zone is formed because here in the cylindrical section the swirl prevents flow separation. Other illustrations of the flow structure are presented in Figs. 9a and 9b, where the distributions of u_e and the displacement thickness are shown, respectively.

Thus, one can see that the semi-inverse method can be used to analyze rather complex flow structures.

Bypass Flow

Simulation of Viscous Zones

The schematic diagram of the bypass flow is presented in Fig. 10. Two streams in a plane channel, initially divided by a splitter, are mixed in a common chamber behind the sharp trailing edge of the splitter. In this flow there are three viscous zones: two separate boundary layers on the channel walls and boundary layers on the splitter walls that form the mixing layer behind the sharp trailing edge. These viscous zones are divided by two potential cores. Viscous zones are assumed to be thin, i.e., all preceding restrictions are valid.

To calculate the boundary layers on channel walls, Eqs. (1-6) must be solved. If the dividing streamlines behind the trailing edge are introduced, the viscous flow along this line is also described by Eqs. (1-3). However, there are some differences in the boundary conditions and the closure relationship.

Upstream of the trailing edge, the boundary conditions have the form (4) for each boundary layer on the upper and lower surfaces of the splitter. Downstream of the trailing edge, the continuity conditions on the dividing streamline must be prescribed, which are given by

$$Y = 0 \quad U_u = U_d \qquad \frac{\partial U_u}{\partial Y} = -\frac{\partial U_d}{\partial} \qquad (27)$$

$$(\nu_t)_u = (\nu_t)_d \; V_u = V_d = 0$$

The asymptotic conditions at $Y \to \infty$ are the same as those upstream of the trailing edge. The boundary conditions on the derivatives of U (where a minus sign occurs because the Y axes have opposite directions above and below the dividing streamline) ensure pressure continuity across the mixing layer. On the other hand, when the inverse problem is considered, the pressure distribution is unknown, so that upstream of the trailing edge two displacement thicknesses must be prescribed, but downstream of the edge only one value is needed. Thus, upstream of the trailing edge closure relationships have the form of Eq. (6), and downstream,

$$\int_0^\infty [1 - \rho U/(\rho_e)_d (U_e)_d]\, dY + mn \int_0^\infty [1 - \rho U/(\rho_e)_u (U_e)_u]\, dY = \delta_m^*(X) \tag{28}$$

Here the $\delta_m^*(X)$ is the displacement thickness for the mixing layer, which may be determined as

$$\delta_m^* = \lim_{y \to \infty} \left\{ \int_\infty^y [1 - \rho U/(\rho_e)_d (U_e)_d]\, dY - (1 - mn) y \right\}$$

where y is the ordinary Cartesian coordinate, m the longitudinal velocity ratio upstream of the trailing edge, and n the density ratio in the mixing streams.

It should be noted that along with the mixing of identical fluids, the mixing of two different fluids may be considered. In the latter case density is a function of the concentration of one of the mixing components

$$c[\rho/(\rho_e)_u] + (1 - c)\,[\rho/(\rho_e)_d] = 1 \tag{29}$$

The concentration c is satisfied by the equation

$$\rho U \frac{\partial c}{\partial X} + \rho V \frac{\partial c}{\partial Y} = \frac{\partial}{\partial Y}\left[\rho(\nu_t/Sc_t + \nu/Sc)\frac{\partial c}{\partial Y}\right] \tag{30}$$

where laminar and turbulent Schmidt numbers (Sc and Sc_t) are assumed to be equal to 0.8.

The boundary conditions are

$$Y \to \infty \quad \frac{\partial c}{\partial Y} = 0; \quad Y = 0 \quad X \le X_{te} \quad \frac{\partial c}{\partial Y} = 0$$
$$Y = 0 \quad X \ge X_{te} \quad C_u = C_d \tag{31}$$

where X_{te} is at the trailing edge. At the initial station $c = 0$ below the splitter and $c = 1$ above the splitter.

Finally, one modification of the turbulence model in the mixing layer is needed, which concerns the last term on the right-hand side of Eq. (3). The distance from the wall must be replaced by the distance from the trailing edge.

Viscous/Inviscid Interaction

The flows in each potential core, above and below the splitter, may be calculated in the same way as in a single channel, i.e., using Eq. (8).

In the general case, the viscous/inviscid interaction between three viscous zones must be considered. However, in this work only wide channels were considered, in which the upper and lower walls were far enough away from the splitter that the influence of the wall's boundary layers on the viscous zone around the splitter may be ignored. The channel walls were assumed parallel to the x axis and the boundary layers were not taken into account.

Two matching conditions, presented by Eq. (9), allow a solution for the displacement thicknesses of the boundary layers above and below the splitter, the thickness of the mixing layer δ_m^*, and the position of the dividing streamline r_∞. The modified Carter's formula was used to obtain the solution. This interaction algorithm may be written as

$$\delta_{u,d}^{*\,i+1}/\delta_{u,d}^{*\,i} = 1 + \zeta_0 \Delta U_{u,d}^i \quad X \le X_{te}$$
$$\delta_m^{*\,i+1}/\delta_m^{*\,i} = 1 + \zeta_1 \Delta U_d^i + \zeta_2 \Delta U_u^i \quad X \ge X_{te} \tag{32}$$
$$r_\infty^{i+1}/r_\infty^i = 1 + \zeta_3 \Delta U_d^i + \zeta_4 \Delta U_u^i$$

where $\Delta U = (u_e - U_e)/U_e$. Our calculations show convergence for all cases if $0 < \xi_0, \xi_1, \xi_2 < 1$; $0 \le \xi_3, \xi_4 \le 0.03$.

Numerical Results

To verify the interaction procedure, a laminar flow near the trailing edge of a flat plate was considered. As the calculations show, when the distance between the flat plate and the channel walls is more than $h/L \ge 2$ (L is plate length) the position of the walls do not influence the flow near the plate. Thus, our results may be compared with data for freestream flow near the trailing edge. The latter was investigated by many authors, and here the results are compared with Veldman's data.[5]

If the origin of the coordinate system is placed at the plate trailing edge, the computational domain is extended from $x/L = -0.5$ to 0.5. The Reynolds number is $Re = 10^5$. Computed results are compared with Veldman's results in Fig. 11, where the wall shear stress and displacement thickness are shown. The agreement is rather good. It should also be noted that in our calculations the symmetry of flow was not assumed a priori, but was predicted as a result.

The next example is a bypass flow in a channel with a deflected flap (see Fig. 10) The contour of the splitter is formed by a line parallel to the x axis and a piece of line with length L inclined to the x axis at angle α, where α is to be assumed small. The corner between the two straight parts is smoothed by a circular arc of radius L. The channel walls are placed at $h_1/L = h_2/L = 1$.

The laminar and turbulent flows in such a channel were considered. For laminar flow the deflected angle α is varied between $0 \le \alpha \le 5$ deg, the velocity ratio at the channel entrance between $0.5 \le m \le 2$, and Reynolds number $Re = L \cdot (U_e)_d/\nu$ between $10^4 \le Re \le 4 \times 10^4$.

The origin of the coordinate system was placed at the trailing-edge station and the computational domain was extended from $x/L = -2$ to 2. The initial parameter distributions are the same as in the boundary layer on a flat plate at the station located at $x/L = 1.0$ from the origin.

The characteristic longitudinal velocity profiles and dividing streamlines for the bypass flow are presented in Fig. 10. These distributions correspond to the regime with $\alpha = 5$ deg, $m = 0.5$, $Re = 10^4$. Before the flap ($x/L = -1$) the velocity profile is a typical boundary-layer profile, just downstream of the trailing edge ($x/L = 0.05$) it is a wake profile, and farther downstream ($x/L = 2$) the velocity profile is a typical mixing layer profile. In the regime considered, separation takes place near the trailing edge. The separation influences the position of the dividing streamline rather strongly, and this influence may be seen in Fig. 10 where the dividing streamlines in

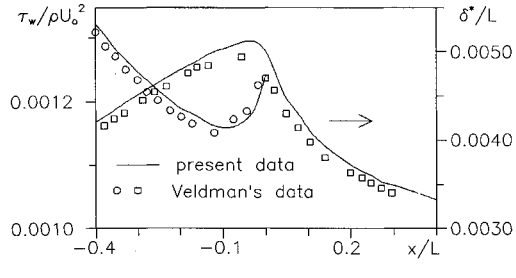

Fig. 11 Wall shear stress and displacement thickness distributions near the trailing edge of a flat plate.

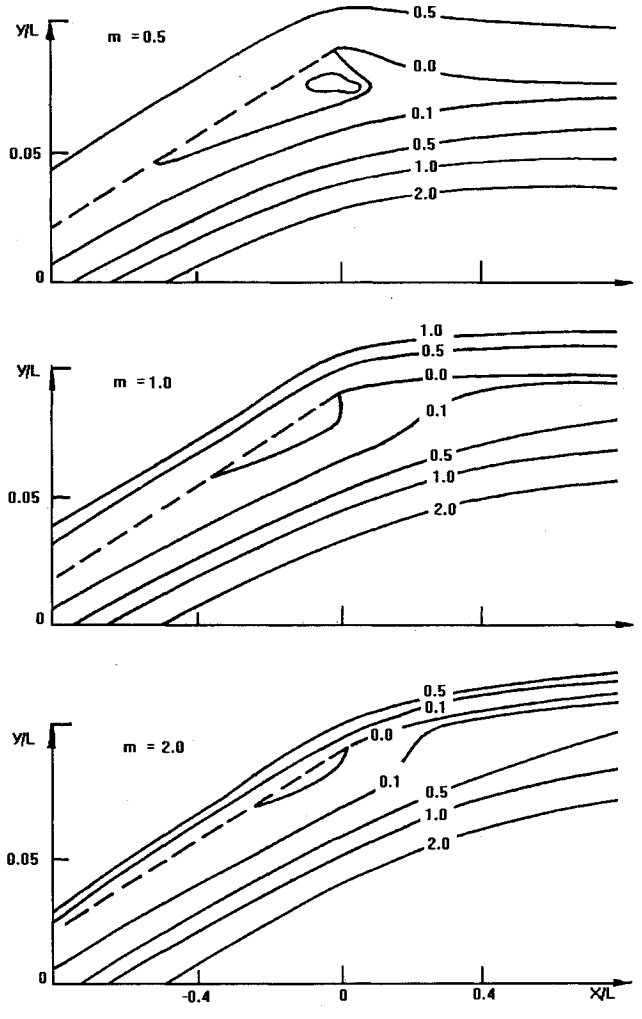

Fig. 12 Map of streamlines around deflected flap at $\alpha = 5$ deg, $Re = 10^4$ (numbers on plot are the values of $[\psi/(u_o L)] \times 10^3$).

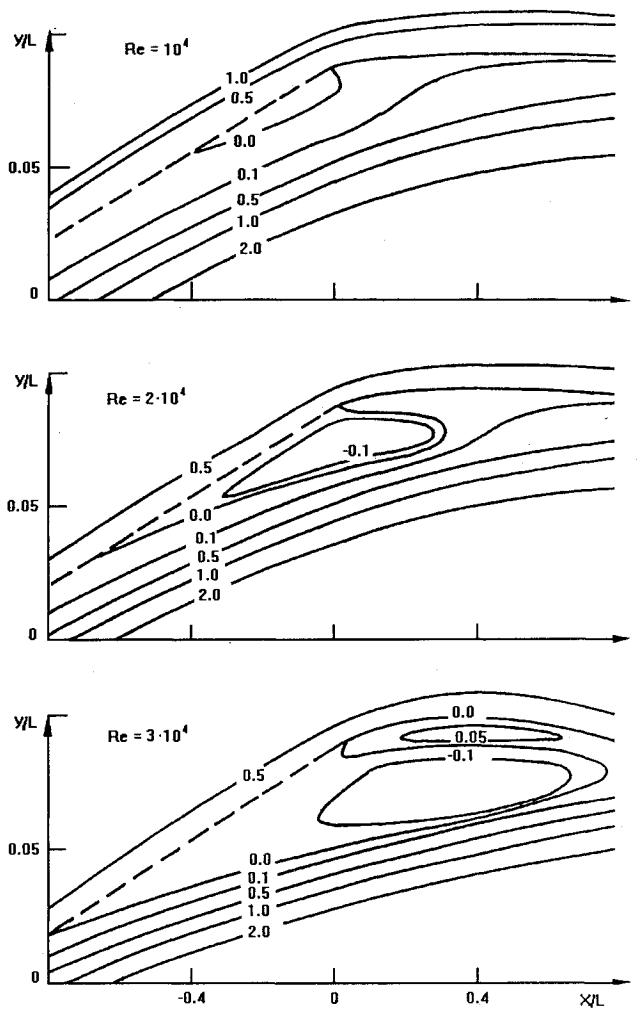

Fig. 13 Map of streamlines around deflected flap at $\alpha = 5$ deg, $m = 1.0$ (numbers on plot are the values of $[\psi/(u_o L)] \times 10^3$).

viscous and inviscid flows (dashed and dashed-dotted curves) are compared. When separation takes place, the dividing streamline moves to the side of the separation zone.

The separation zones have the streamline patterns shown in Figs. 12 and 13, which also illustrate the influence of the flow regime on the flow structures. In Fig. 12, the influence of velocity ratio m is presented ($\alpha = 5$ deg, $Re = 10^4$). When m is increased the size of the separation zone is diminished because the separation point moves downstream. Thus, in a bypass flow by varying the velocity in one part of a channel, one can control the separation in another part. When m is increased the dividing streamline is close to such a line in an inviscid flow, but if m is decreased the dividing streamline moves down and the bypass ratio (the ratio of flow rates) is decreased by more than m.

In Fig. 13, the influence of the Reynolds number is presented ($\alpha = 5$ deg, $m = 1$). When Re is increased the separation zone is increased, the separation point moves upstream, and the reverse flow zone intrudes into the mixing layer. When the primary recirculation zone intrudes into the mixing layer, a secondary recirculation zone arises. Analogous changes in structure take place when the Reynolds number is fixed, but the deflection angle α is increased.

Finally, laminar and turbulent bypass flows, characterized by $\alpha = 5$ deg, $m = 1$, were compared. In Fig. 14 the wall shear stress distributions below the splitter in the laminar ($Re = 10^4$) and turbulent ($Re = 10^4$) flows are presented (in both the laminar and turbulent cases initial displacement thicknesses δ_o^* were equal). In the turbulent flow, the size of the separation

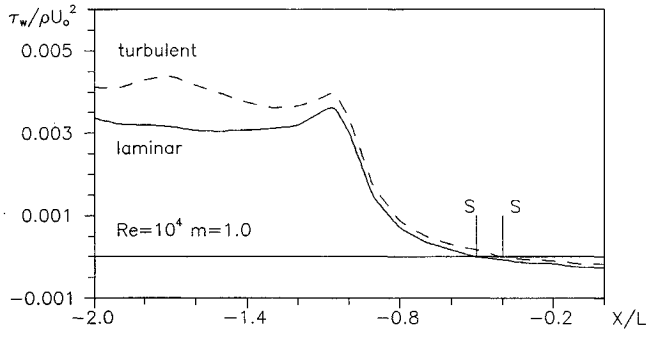

Fig. 14 Comparison of wall shear stress distributions along the deflected flap in laminar and turbulent flows.

zone is diminished because the effective Reynolds number, computed using the turbulent viscosity, is decreased. The streamline pattern in the turbulent case is analogous to the pattern in the laminar case.

Concluding Remarks

The interaction boundary-layer algorithm for effective simulation of separated duct flows was developed.

It was shown that calculated results for laminar flows in a plane duct were in good agreement with known theoretical data. The calculated results for turbulent flows also agree well

with experimental data. The improved interaction formula decreases the required number of iterations by about 30% compared with Carter's formula.

The influence of swirl on a separated flow in an annular duct was investigated by the present method. A new type of self-similar solution of the swirl boundary-layer equations was also found.

It was shown that rather strong swirl induces boundary layer separation on the convex cylindrical surface and accelerates the flow on the concave cylindrical surface. On an inclined surface, when the velocity of the mainstream is directed toward the axis of symmetry, the flow accelerates but if the main flow is directed outward the stream decelerates and may separate.

Finally, the bypass flow with a strong viscous/inviscid interaction near the trailing edge of the stream splitter was considered. The influences of velocity ratio and Reynolds number on the separated zone structure were investigated. It was shown that velocity changes at one stream entrance may control the separation in the other stream. It was also shown that when the Reynolds number is increased, two separation bubbles occur, one downstream at the trailing edge of the splitter. The laminar and turbulent regimes with equal Reynolds numbers were compared and it was shown that tripping to achieve a turbulent flow prevents separation near the trailing edge of the splitter.

Acknowledgment

The author thanks S. V. Hohlov, who performed some calculations and took part in discussion of the problem.

References

[1]Catherall, D., and Mangler, K. W., "The Integration of the Two-Dimensional Laminar Boundary Layer Equations Past the Point of Vanishing Skin Friction," *Journal of Fluid Mechanics,* Vol. 26, Sept. 1966, pp. 163–182.

[2]Carter, J. E., "Solution for Laminar Boundary-Layers with Separation and Reattachment," AIAA Paper 74-583, June 1974.

[3]Anon., *Numerical and Physical Aspects of Aerodynamic Flows,* edited by T. Cebeci, Springer-Verlag, New York, 1982, p. 636.

[4]Anon., *Numerical and Physical Aspects of Aerodynamic Flows, II,* edited by T. Cebeci, Springer-Verlag, New York, 1984, p. 416.

[5]Veldman, A. E. P., "New, Quasi-simultaneous Method to Calculate Interacting Boundary Layers," *AIAA Journal,* Vol. 19, No. 1, 1981, pp. 79–85.

[6]Abramovitch, G. N., Krasheninnikov, S. Ju., and Sekundov, A. N., "Turbulent Flows with Volume Forces and Nonsimularity," *Moscow, Mashinostroienie,* 1975, p. 96 (in Russian).

[7]Hinze, J. O., *Turbulence,* McGraw-Hill, New York, 1975, p. 790.

[8]Reyhner, T. A., and Flugge-Lotz, I., "The Interaction of a Shock Wave with a Laminar Boundary Layer," *International Journal of Non-Linear Mechanics,* Vol. 3, No. 2, 1968, pp. 173–199.

[9]Blottner, F. G., "Variable Grid Scheme Applied to Turbulent Boundary Layers," *Computer Methods in Applied Mechanics and Engineering,* Vol. 4, No. 2, 1974, pp. 179–194.

[10]Vasilev, V. I., Hohlov, S. V., and Shalman, E. Ju., "On Calculation Separated Flows Using Boundary Layer Equations," *Zurnal prikladnoi mechaniki i tekhnicheskoi fiziki,* No. 6, 1990, pp. 46–54 (in Russian).

[11]Simpson, R. L., Chew, Y. T., and Shivaprasad, B. G., "The Structure of Separating Turbulent Boundary Layer, Pt. 1, Mean Flow and Reynolds Stresses," *Journal of Fluid Mechanics,* Vol. 113, Dec. 1981, p. 23.

[12]Halim, A., and Hafez, M., "Calculation of Separation Bubbles Using Boundary-Layer Type Equations," *AIAA Journal,* Vol. 24, No. 4, 1986, pp. 585–590.

[13]Serpa, J. M., Lessman, R. C., and Hagist, W. M., "Turbulent Separated and Reattached Flows over a Curved Surface," AIAA Paper 86-1064, May 1986.

[14]Back, L. H., "Flow and Heat Transfer in Laminar Boundary Layers with Swirl," *AIAA Journal,* Vol. 8, No. 9, 1969, pp. 1781–1789.